Zinc-Ion Batteries

International Edition: DOI: 10.1002/anie.201713291
German Edition: DOI: 10.1002/ange.201713291

Highly Stable Aqueous Zinc-Ion Storage Using a Layered Calcium Vanadium Oxide Bronze Cathode

*Chuan Xia[+], Jing Guo[+], Peng Li, Xixiang Zhang, and Husam N. Alshareef**

Abstract: *Cost-effective aqueous rechargeable batteries are attractive alternatives to non-aqueous cells for stationary grid energy storage. Among different aqueous cells, zinc-ion batteries (ZIBs), based on Zn^{2+} intercalation chemistry, stand out as they can employ high-capacity Zn metal as the anode material. Herein, we report a layered calcium vanadium oxide bronze as the cathode material for aqueous Zn batteries. For the storage of the Zn^{2+} ions in the aqueous electrolyte, we demonstrate that the calcium-based bronze structure can deliver a high capacity of 340 mA h g^{-1} at 0.2 C, good rate capability, and very long cycling life (96 % retention after 3000 cycles at 80 C). Further, we investigate the Zn^{2+} storage mechanism, and the corresponding electrochemical kinetics in this bronze cathode. Finally, we show that our Zn cell delivers an energy density of 267 W h kg^{-1} at a power density of 53.4 W kg^{-1}.*

Aqueous rechargeable batteries are a promising class of batteries for grid-scale electrochemical energy storage.[1] This is largely because of their low cost and high operational safety. Further, it is well known that aqueous electrolytes offer much higher ionic conductivities (ca. 1 S cm^{-1}), compared to non-aqueous electrolytes (ca. 1–10 mS cm^{-1}), which favors high rate capabilities.[2] Efforts in large-scale aqueous energy storage has spanned naturally abundant Na^+ and K^+ intercalation materials,[3] as well as multivalent charge carriers (e.g., Zn^{2+}, Ca^{2+}, Mg^{2+}, and Al^{3+}).[4] Obviously, rechargeable cells employing multivalent ions can, in principle, deliver higher storage capacity due to multiple electron transfers. Among them, aqueous zinc-ion batteries (ZIBs), based on Zn^{2+} intercalation chemistry, stand out owing to the following properties of Zn anodes: 1) high capacity (820 mA h g^{-1}; 5851 mA h mL^{-1}); 2) high abundance and low cost;[1b] 3) low redox potential (−0.76 V vs. standard hydrogen electrode);[5] and 4) impressive electrochemical stability in water due to a high overpotential for hydrogen evolution.[2] Moreover, replacement of the alkaline electrolyte by mild neutral pH (or slightly acidic) solution can virtually eliminate the issues of dendritic zinc, which prevail in alkaline zinc cells, and simultaneously decrease the environmental impact and maintenance cost.[6] One of the main challenges which hinder the practical application of aqueous ZIBs is the lack of suitable intercalation cathodes, which can offer high capacity and good structure stability during Zn^{2+} (de)intercalation. Thus, the development of high-performance ZIB cathode is a prerequisite to achieve stable aqueous zinc-ion storage.

In the early stages of development, polymorphs of MnO_2 were seriously investigated as potential Zn^{2+} host materials.[1a,7] Afterwards, Prussian blue analogues were proposed to realize stable aqueous ZIBs.[8] Unfortunately, these electrodes suffer from either limited capacity or very poor cycling stability. Very recently, layered and hydrated V_2O_5 derivatives (e.g. $Zn_{0.25}V_2O_5{\cdot}n\,H_2O$)[2] were reported as high-performance ZIB cathodes, which delivered high capacity (> 300 mA h g^{-1}) and long-term cycling stability (> 1000 cycles), as well as impressive rate capability. Such improvements in performance were mainly attributed to the following: 1) Their open-framework crystal structure with pillars between V_2O_5 bilayers (leading to expanded interlayer spacing), which insures fast and reversible Zn^{2+} insertion/removal. In addition, compared with monovalent alkali metal cations (e.g. Li^+, Na^+, K^+), the divalent metal ions bonded with oxygen atoms can bring about stronger ionic bonds,[9] better binding the layers together, which effectively prevents structural collapse; 2) The tendency of vanadium to exist in multiple oxidation states, hence making it high capacity in principle; 3) The charge shield effect of the crystal H_2O, which could reduce the effective charges of intercalated Zn^{2+} ions, and thus enhance the capacity and rate performance.[6,10] To capitalize on these features, herein, we propose double-layered calcium vanadium oxide bronze ($Ca_{0.25}V_2O_5{\cdot}n\,H_2O$ or CVO) as a more suitable aqueous ZIB intercalation cathode than $Zn_{0.25}V_2O_5{\cdot}n\,H_2O$ based on the following considerations: 1) Compared to the ZnO_6 octahedra pillars in $Zn_{0.25}V_2O_5{\cdot}n\,H_2O$, the larger CaO_7 polyhedra in CVO may further expand the size of the cavity between V_4O_{10} layers; 2) The lower molecular weight and density of CVO probably can give higher gravimetric and volumetric capacity; 3) CVO offer fourfold higher electrical conductivity than $Zn_{0.25}V_2O_5{\cdot}n\,H_2O$, as demonstrated later. We show that the freestanding CVO paper cathode deliver capacities of 340 and 289 mA h g^{-1} at 0.2 and 1 C, respectively. The fast electrochemical kinetics of CVO is also quantitatively illustrated using cyclic voltammetry. We demonstrate that, even when cycled at 80 C, the CVO cathode retains ca. 96 % and ca. 78 % of its initial capacity after 3000 and 5000 cycles, respectively. A highly reversible Zn^{2+} intercalation mechanism is elucidated using ex situ X-ray diffraction (XRD), X-ray photo-

[*] C. Xia,[+] J. Guo,[+] Dr. P. Li, Prof. X. X. Zhang, Prof. H. N. Alshareef
Materials Science and Engineering
King Abdullah University of Science and Technology (KAUST)
Thuwal 23955-6900 (Saudi Arabia)
E-mail: husam.alshareef@kaust.edu.sa
[+] These authors contributed equally to this work.
Supporting information and the ORCID identification number(s) for the author(s) of this article can be found under: https://doi.org/10.1002/anie.201713291.

electron spectroscopy (XPS), and transmission electron microscope (TEM) studies.

The CVO sample was synthesized using a one-step hydrothermal method (see the Supporting Information for details). As shown in Figure 1a and Figure S1, the crystal structure of CVO is very similar to that of δ-type $Zn_{0.25}V_2O_5{\cdot}n\,H_2O$.[11] Common to both of these oxides is that the V_2O_5 layers stack along the *c* axis and the intercalated metal ions (Zn^{2+} or Ca^{2+}) as well as water molecules reside in the interlayer space.[12] The intercalated metal ions can strongly bond to V_2O_5 layers and H_2O to form polyhedra pillars (ZnO_6 and CaO_7), which expand the interlayer gap of V_2O_5 and make the formed crystal more stable. However, the Ca–O bonds in CaO_7 pillars (2.38–2.57 Å)[12] are much longer than Zn–O bonds (2.03–2.13 Å)[11] in $Zn_{0.25}V_2O_5{\cdot}n\,H_2O$, implying that an increased interlayer space is expected for the CVO crystal. The XRD analysis supports our hypothesis. As displayed in Figure 1b, the XRD pattern of pristine CVO is dominated by (00*l*) reflections, revealing a high degree of preferred orientation along the *c* axis. Further, the absence of any impurity peaks demonstrates the single-phase nature of as-prepared CVO. In CVO the downshift of the diffraction angle corresponding to (00*l*) peaks compared to $Zn_{0.25}V_2O_5{\cdot}n\,H_2O$ confirms its larger interlayer distance along (00*l*) direction. We also found that the V_2O_5 open framework of CVO allows the insertion of water molecules from the electrolyte into its interlayer space, in agreement with a previous report.[2] The XRD result (Figure 1c) indicates that the interlayer space of CVO increased from 10.6 to 14.1 Å upon immersion in electrolyte, corresponding to water intercalation. Of note, the pristine XRD pattern can be recovered by vacuum drying. Apparently, more water molecules can be intercalated into the CVO lattice (3.5 Å increase of interlayer space) than in $Zn_{0.25}V_2O_5{\cdot}n\,H_2O$ (2.3 Å increase of interlayer space), confirming a more open crystal structure for CVO. This feature may facilitate the electrochemical (de)intercalation of Zn^{2+} ions into CVO crystal. Inductively coupled plasma optical emission spectroscopy

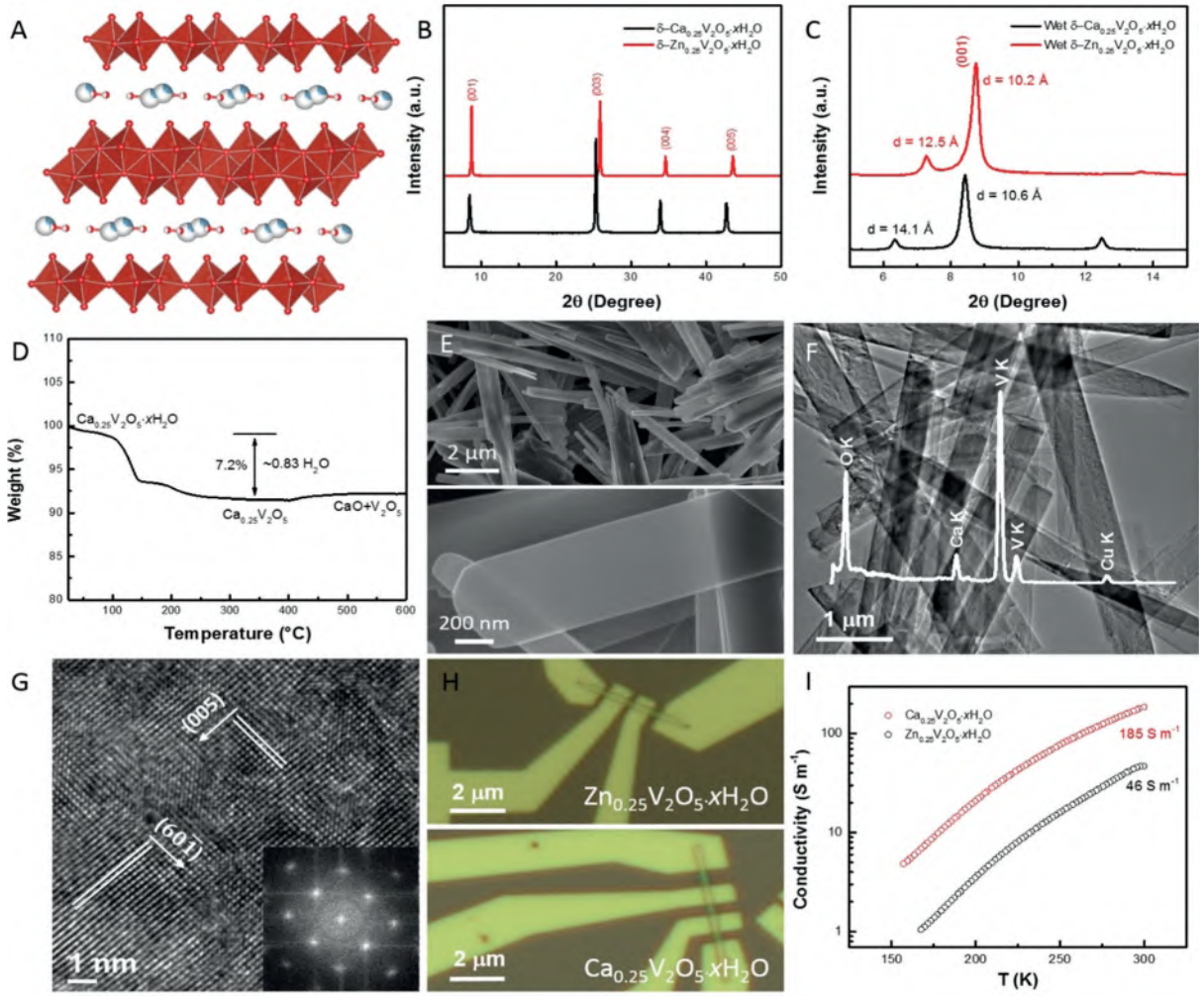

Figure 1. A) Crystal structure viewed along the *b*-axis of CVO, which shows a double-layered structure with an open framework. The V atoms in V_2O_5 polyhedra are depicted in red. The blue/white and red/white atoms in the crystal represent the intercalated Ca ions and lattice water, respectively. B, C) Typical XRD pattern of as-synthesized CVO. D) TGA results for CVO samples. E–G) SEM and TEM images of CVO nanobelts. Inset in (F) shows the EDS spectrum of as-obtained CVO, showing the existence of O, Ca, and V elements. The Ca/V atomic ratio is ca. 0.13. H) The individual CVO and $Zn_{0.25}V_2O_5{\cdot}n\,H_2O$ based nanodevices, and I) their corresponding electricity conductivities.

(ICP-OES) and thermogravimetric (TGA) studies (Figure 1 d) further reveal that the stoichiometric formula for the as-prepared calcium vanadium oxide bronze is $Ca_{0.24}V_2O_5{\cdot}0.83\,H_2O$.

Scanning electron microscope (SEM) images reveal a typical nanobelt morphology with a smooth surface for as-synthesized CVO (Figure 1 e); the nanobelts are shown to be a few micrometers long and several hundred nanometers wide. The representative TEM images (Figure 1 f,g) further illustrate the flat ribbon morphology and single-crystallinity of CVO materials. A lattice fringe with d-spacing of 0.196 and 0.211 nm can be observed in the high-resolution TEM image, corresponding to $(60\bar{1})$ and (005) planes of CVO nanobelt, respectively. The elemental composition of the nanobelt was investigated by energy-dispersive X-ray spectroscopy (EDS) (inset in Figure 1 f) and the result shows that the atomic ratio of Ca to V is ca. 0.13, which is close to that of $Ca_{0.24}V_2O_5{\cdot}0.83\,H_2O$. Additionally, we show that the CVO nanobelts are typically 50–60 nm thick, as determined by atomic force microscopy (Figure S2). Considering the importance of the electrical conductivity of electrode materials for energy-storage applications, we then precisely measured the electrical conductivities of as-prepared samples using individual nanobelt-based nanodevices (Figure 1 h). As shown in Figure 1 i, the CVO sample offers a fourfold higher electrical conductivity than that of the previously reported $Zn_{0.25}V_2O_5{\cdot}n\,H_2O$ nanobelt at room temperature. Undoubtedly, the higher electrical conductivity can boost the electron transfer during Zn^{2+} (de)intercalation, thereby enhancing battery performance.

The freestanding CVO paper electrode was used as the cathode in an aqueous ZIB, where the zinc metal and 1.0 M $ZnSO_4$ aqueous solution served as anode and electrolyte, respectively. The CVO paper electrode (ca. 5.7 mg cm^{-2}) was prepared using a vacuum-filtration method (see the Experimental Section in the Supporting Information). The Zn//CVO cells were cycled in a voltage window of 0.6–1.6 V versus Zn, considering the structural stability of cathode materials. As shown in Figure S3a, in such a voltage window the Zn cell is very robust. Figure S3b shows the 1st, 2nd, 5th, and 10th cycles of the cyclic voltammetry (CV) curves recorded at a scan rate of 0.1 mV s^{-1}. Multiple pairs of redox peaks are observed, demonstrating a multistep reaction mechanism associated with Zn^{2+} insertion/extraction. The CV study implies that the Zn^{2+} (de)intercalation process in the Zn//CVO cell is highly reversible since no obvious peak current losses are observed between the 2nd and 10th CV scans. Figure 2 a shows the galvanostatic charge-discharge (CD) profiles at various current densities. A high initial capacity of 340 mA h g^{-1} is achieved at 0.2 C. The predominantly sloping CD curves suggest fast kinetics which originate from the solid-solution type process. To further understand the electrochemical kinetics of CVO cathode, we quantified the capacitive and diffusion limited contributions to the total capacity using previously reported approach by Dunn and co-workers.[13] Figure 2 b exhibits the CV curves of CVO electrode from 0.2 to 0.5 mV s^{-1}. With increasing scan rates, the CV curves maintain the same shape with subtle shifting of redox peaks. The results, summarized in Figure 2 c, show that at a scan rate of 0.3 mV s^{-1}, 76 % of the current can

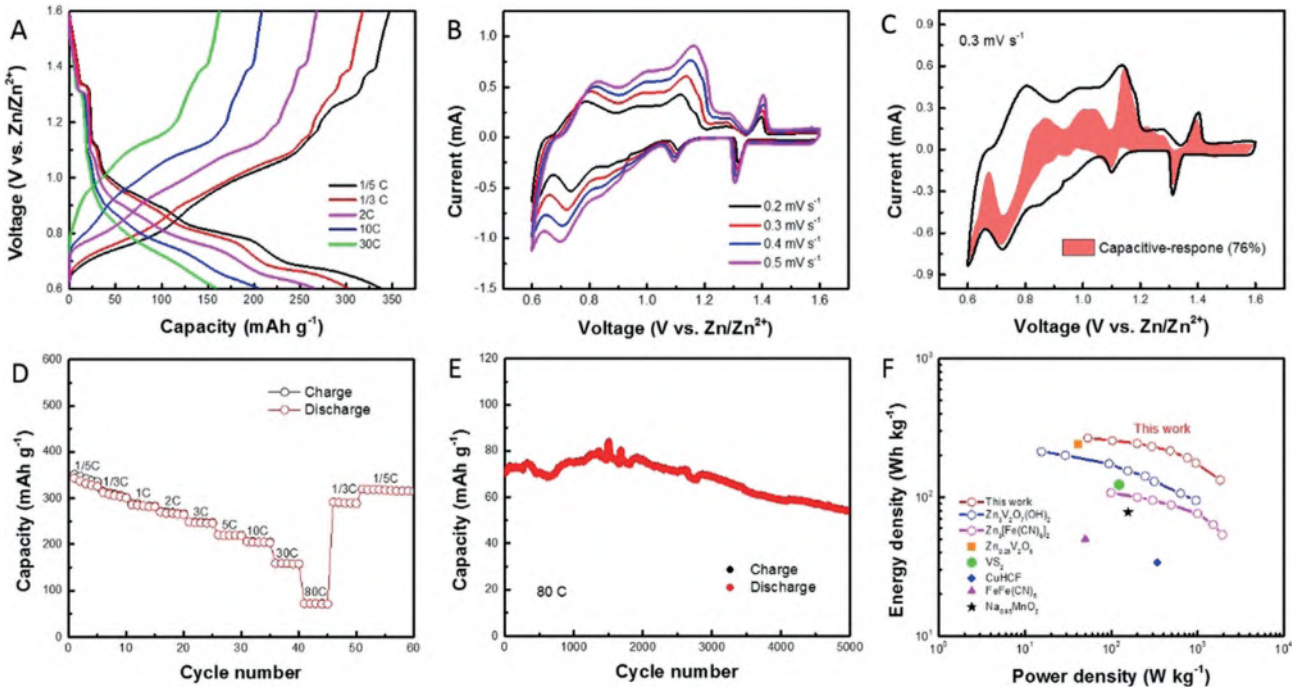

Figure 2. A) Galvanostatic charge–discharge profiles for CVO electrodes at different current densities. B) Cyclic voltammetry curves of CVO electrodes recorded at various scan rates. C) Capacity separation analysis at 0.3 mV s^{-1}. The red-shaded data show the contribution to capacitive charge storage as a function of potential. D) Rate performance of CVO cathodes. E) Cycle performance at a current rate of 80 C. F) The Ragone plot of Zn//CVO cell in comparison with other aqueous ZIBs.

be attributed to the capacitive response of the CVO cathode, clearly indicating that the corresponding solid-solution reactions are mainly limited by the electrochemical reaction rate itself instead of the mobile-ion diffusion rate. Further, we employed the galvanostatic intermittent titration technique (GITT) to estimate the Zn^{2+} ion diffusion coefficient in CVO cathode (see details in Figure S4). Despite the divalent nature of the Zn^{2+} ion, the GITT-determined diffusion coefficient is still as high as ca. 10^{-8} to 10^{-9} $cm^2 s^{-1}$.The above discussion clearly demonstrates the fast kinetics of as-prepared CVO materials, and supports their good rate capability.

The rate performance of our CVO cathode is illustrated in Figure 2d, where the current density was increased stepwise from 0.2 to 80 C and returned to 0.2 C. It is obvious that the CVO electrodes retain 85% of the initial specific capacity when the current increases from 0.2 (340 mA h g^{-1}) to 1 C (289 mA h g^{-1}), outperforming previously reported $Zn_{0.25}V_2O_5{\cdot}nH_2O$ (300 and 282 mAh g^{-1} at 1/6 and 1 C, respectively). Even at a fast charge–discharge rate of 80 C (45 s), these CVO electrodes still offer a high capacity of 72 mA h g^{-1} due to the fast Zn^{2+} ion migration. Of note, the capacity of these CVO electrodes recovered to 323 mA h g^{-1} (95%) when the current density was returned to 0.2 C, suggesting excellent structural stability. We also note that the CVO cathodes do not show notable capacity decay over at least 3000 cycles (ca. 96% retention) even at very high current density of 80 C (Figure 2e). In contrast, the $Zn_{0.25}V_2O_5{\cdot}nH_2O$ cathode show 19% capacity decay only after 1000 cycles at 8 C rate.[2] It is worthwhile to note that the Columbic efficiency of the CVO cathode during cycling tests is close to 100%, confirming that the impressive cycling performance is not due to parasitic reactions. Figure 2f shows the Ragone plot of our Zn//CVO cell, in comparison to other reported intercalation Zn cells. Impressively, our devices show a very high energy density of 267 W h kg^{-1} at a power density of 53.4 W kg^{-1}. Even the cell is charged within 45 s, the energy density is still as high as 133 W h kg^{-1} at an outstanding power density of 1825 W kg^{-1}. Furthermore, it can be seen that our cells offer better performance than cells based on $Zn_3V_2O_7(OH)_2$,[14] $Zn_{0.25}V_2O_5{\cdot}nH_2O$,[2] $Zn_3[Fe(CN)_6]_2$[8a] CuHCF,[8b] VS_2,[15] $FeFe(CN)_6$,[16] and $Na_{0.95}MnO_2$[17] cathodes.

The successful and stable aqueous storage of Zn^{2+} in the CVO cathode can be demonstrated by ex situ high-resolution XPS analysis. As shown in Figure 3a, there is no Zn signal in the initial state for CVO cathode. However, the Zn 2p peaks ($2p_{3/2}$: 1022 eV)[18] emerge when the CVO electrodes were

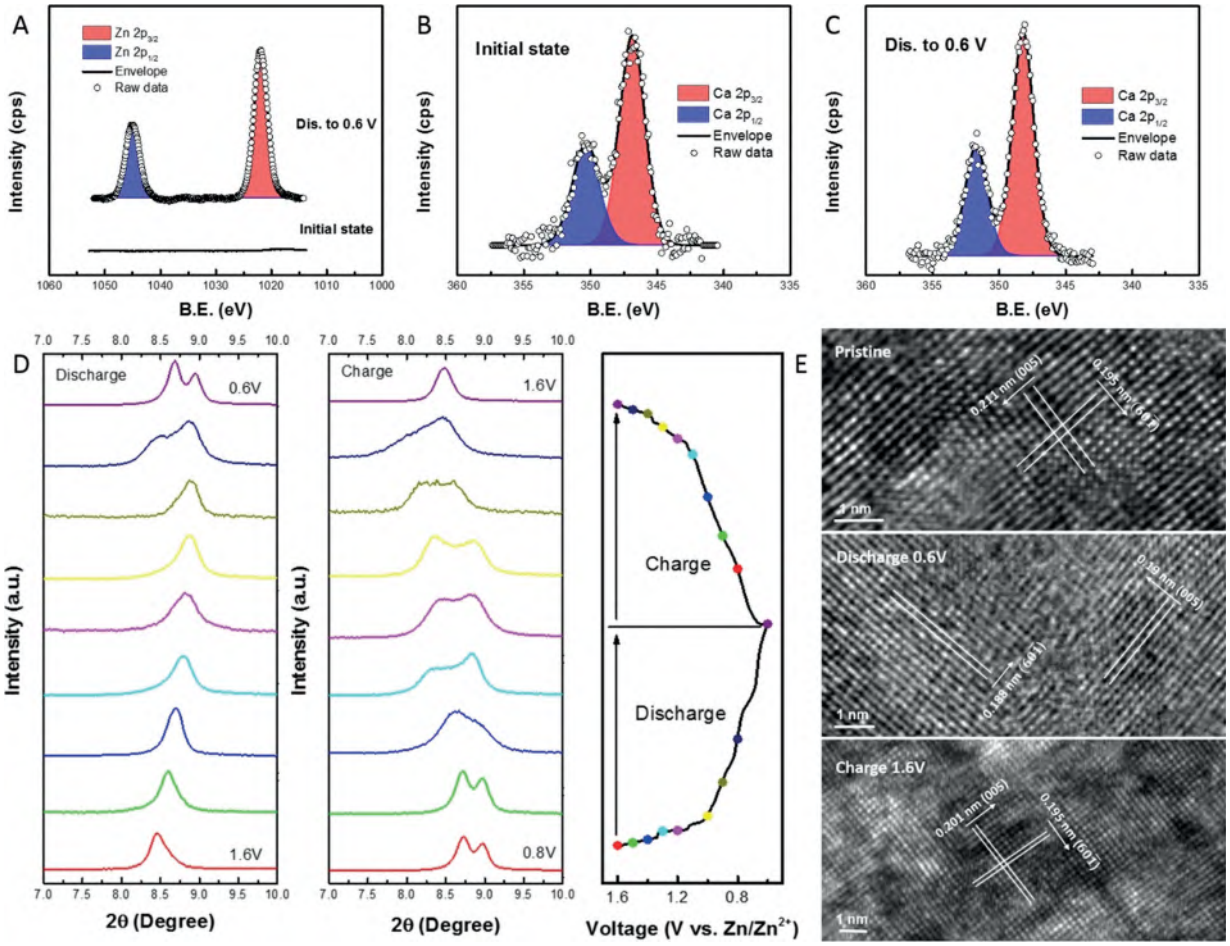

Figure 3. Ex-situ high-resolution XPS spectra of the A) Zn 2p and B,C) Ca 2p regions in pristine and fully discharged state of the CVO electrodes. D) Ex-situ XRD patterns of (001) Bragg peak of the CVO cathode 3rd charge-discharge scan as a function of discharge and charge voltage. E) Ex-situ high-resolution TEM images of the CVO nanobelt at initial, fully discharged (0.6 V) and charged state (1.6 V).

discharged to 0.6 V. The newly evolved Zn peaks clearly demonstrate the successful insertion of Zn^{2+} ions into the porous CVO lattice. Next, we show that the CaO_7 pillars are quite stable during Zn^{2+} incorporation. Specifically, we do not observe any intensity decrease for Ca 2p peaks as we go from the initial state to the fully discharged state (Figure 3b,c). Further, it is worth noting that fully discharged CVO electrode shows only one Ca 2p component (Ca^{2+}), implying that the CaO_7 pillars are not partially reduced as a consequence of $Zn^{2+}/2e^-$ intercalation. The blueshift (346.9 eV for pristine CVO; 348.1 eV for discharged state) of the binding energy for the Ca^{2+} component in the fully discharged CVO cathode is linked to the intercalation of the Zn^{2+} ions. A very similar blueshift was previously observed in a Cr-intercalated $CaCO_3$ system.[19] In order to gain better insight into the electrochemical process during Zn^{2+} (de)intercalation, ex situ XRD analysis was carried out. Figure S5 shows that (00*l*) Bragg peaks corresponding to the CVO phase shift to higher angles in the fully discharged state (0.6 V), and nearly return to their initial positions upon discharge to 1.6 V. Apparently, the CVO cathode does not undergo a phase evolution following Zn^{2+} insertion and extraction. Typically, the interlayer spacing in the layered intercalation cathode should be expanded after the incorporation of guest ions. However, a small contraction (ca. 5.7%) of the CVO lattice (10.6 Å for (001) planes) is observed upon discharge to 0.6 V (10 Å for (001) planes). This is likely due to the increased screening of the interlayer electrostatic repulsion due to Zn^{2+} insertion and the expulsion of water molecules from between the layers, which has been demonstrated by Nazar and coworkers.[2] Moreover, even after 100 continuous CD cycles, the CVO cathode can perfectly preserve its crystal structure without the formation of impurities, for example, basic zinc sulfate. The 100 times cycled CVO electrode retained a 10.3 Å interlayer spacing, similar to the 10.6 Å interlayer spacing observed in fresh CVO nanobelts, indicating highly reversible Zn^{2+} intercalation in the CVO host without structural breakdown.

Figure 3d displays the evolution of the (001) peak of CVO electrode in detail during the 3rd CD scan. During the discharge process, Zn^{2+} ions are gradually intercalated into the V_4O_{10} double-layers, leading to a contraction of interlayer spacing, which can be immediately recovered upon voltage reversal. This reversibility and gradual shifting of the (001) peak indicates that the related solid-solution process is associated with Zn^{2+} (de)intercalation from the CVO interlayer. We also notice that a peak split appears when CVO is discharged to 0.8 V, which probably results from a dramatic crystal distortion. At 0.6 V, an obvious peak split is observed. While cycling in a wide voltage window resulted in more Zn^{2+} intercalation, the huge structural stress could lead to very fast capacity decay. Thus, 0.6 V is identified as the cut-off voltage for our Zn//CVO cells. About 1.31 Zn ions per CVO unit can be intercalated without apparent crystal breakdown of the CVO. The ex situ high-resolution TEM analysis provides further proof for the unusual Zn^{2+} storage mechanism of CVO cathodes. As shown in Figure 3e, the $(60\bar{1})$ and (005) planes of pristine CVO nanobelts exhibit lattice fringes with d-spacings of 0.195 and 0.211 nm, respectively. When discharged to 0.6 V, a lattice fringe with d-spacings of 0.188 and 0.19 nm is observed, corresponding to $(60\bar{1})$ and (005) planes, respectively. Such a subtle lattice contraction (3.6–9.9%) is consistent with our XRD data. Impressively, the contracted crystal structure immediately recovered to its initial state (0.195 and 0.201 nm for $(60\bar{1})$ and (005) planes, respectively) upon Zn^{2+} ion removal (1.6 V). These findings match those deduced from the ex situ XRD and XPS studies: the CVO nanobelt is a suitable cathode material for stable aqueous Zn-ion storage. Furthermore, considering the abundance and low cost of Ca, Zn, and V, our Zn//CVO cell presents a potentially safe, durable, and cost-efficient device for large-scale energy storage.

We have synthesized calcium vanadium oxide bronze ($Ca_{0.24}V_2O_5{\cdot}0.83\,H_2O$) nanostructures using a one-step hydrothermal method, and used them as aqueous ZIB cathodes. The freestanding CVO paper cathode delivers capacities of 340 and 289 $mA\,h\,g^{-1}$ at 0.2 and 1 C, respectively. Our Zn//CVO cells show an impressive energy density of 267 $W\,h\,kg^{-1}$ at a power density of 53.4 $W\,kg^{-1}$, outperforming most of the previously reported protypes. Excellent cycling stability (up to 5000 cycles at 80 C) and rate capability were also demonstrated. The structural evolution and electrochemical kinetics were discussed in detail. The low cost and excellent lifespan show that nanostructured CVO is a viable cathode for aqueous Zn-ion storage.

Acknowledgements

Research reported in this publication was supported by King Abdullah University of Science and Technology (KAUST).

Conflict of interest

The authors declare no conflict of interest.

Keywords: batteries · calcium vanadium oxide bronze · electrode materials · intercalation · zinc

How to cite: *Angew. Chem. Int. Ed.* **2018**, *57*, 3943–3948
Angew. Chem. **2018**, *130*, 4007–4012

[1] a) C. Xu, B. Li, H. Du, F. Kang, *Angew. Chem. Int. Ed.* **2012**, *51*, 933–935; *Angew. Chem.* **2012**, *124*, 957–959; b) J. F. Parker, C. N. Chervin, I. R. Pala, M. Machler, M. F. Burz, J. W. Long, D. R. Rolison, *Science* **2017**, *356*, 415–418; c) B. J. Hertzberg, A. Huang, A. Hsieh, M. Chamoun, G. Davies, J. K. Seo, Z. Zhong, M. Croft, C. Erdonmez, Y. S. Meng, *Chem. Mater.* **2016**, *28*, 4536–4545.

[2] D. Kundu, B. D. Adams, V. Duffort, S. H. Vajargah, L. F. Nazar, *Nat. Energy* **2016**, *1*, 16119.

[3] a) X. Wu, Y. Cao, X. Ai, J. Qian, H. Yang, *Electrochem. Commun.* **2013**, *31*, 145–148; b) C. D. Wessells, S. V. Peddada, R. A. Huggins, Y. Cui, *Nano Lett.* **2011**, *11*, 5421–5425; c) L. Peng, Y. Zhu, X. Peng, Z. Fang, W. Chu, Y. Wang, Y. Xie, Y. Li, J. J. Cha, G. Yu, *Nano Lett.* **2017**, *17*, 6273–6279; d) H. Li, L. Peng, Y. Zhu, D. Chen, X. Zhang, G. Yu, *Energy Environ. Sci.* **2016**, *9*, 3399–3405; e) Y. Zhu, L. Peng, D. Chen, G. Yu, *Nano Lett.* **2016**, *16*, 742–747.

[4] a) X. Wu, Y. Xiang, Q. Peng, X. Wu, Y. Li, F. Tang, R. Song, Z. Liu, Z. He, X. Wu, *J. Mater. Chem. A* **2017**, *5*, 17990 – 17997; b) H. Zhang, K. Ye, S. Shao, X. Wang, K. Cheng, X. Xiao, G. Wang, D. Cao, *Electrochim. Acta* **2017**, *229*, 371 – 379; c) S. Liu, J. Hu, N. Yan, G. Pan, G. Li, X. Gao, *Energy Environ. Sci.* **2012**, *5*, 9743 – 9746.
[5] G. Li, Z. Yang, Y. Jiang, C. Jin, W. Huang, X. Ding, Y. Huang, *Nano Energy* **2016**, *25*, 211 – 217.
[6] M. Yan, P. He, Y. Chen, S. Wang, Q. Wei, K. Zhao, X. Xu, Q. An, Y. Shuang, Y. Shao, *Adv. Mater.* **2017**, 1703725.
[7] a) H. Pan, Y. Shao, P. Yan, Y. Cheng, K. S. Han, Z. Nie, C. Wang, J. Yang, X. Li, P. Bhattacharya, *Nat. Energy* **2016**, *1*, 16039; b) M. H. Alfaruqi, V. Mathew, J. Gim, S. Kim, J. Song, J. P. Baboo, S. H. Choi, J. Kim, *Chem. Mater.* **2015**, *27*, 3609 – 3620.
[8] a) L. Zhang, L. Chen, X. Zhou, Z. Liu, *Adv. Energy Mater.* **2015**, *5*, 1400930; b) R. Trócoli, F. La Mantia, *ChemSusChem* **2015**, *8*, 481 – 485; c) Z. Jia, B. Wang, Y. Wang, *Mater. Chem. Phys.* **2015**, *149*, 601 – 606.
[9] Y. Ma, H. Zhou, S. Zhang, S. Gu, X. Cao, S. Bao, H. Yao, S. Ji, P. Jin, *Chem. Eur. J.* **2017**, https://doi.org/10.1002/chem.201702814.
[10] E. Levi, Y. Gofer, D. Aurbach, *Chem. Mater.* **2010**, *22*, 860 – 868.
[11] Y. Oka, O. Tamada, T. Yao, N. Yamamoto, *J. Solid State Chem.* **1996**, *126*, 65 – 73.
[12] Y. Oka, T. Yao, N. Yamamoto, *J. Solid State Chem.* **1997**, *132*, 323 – 329.
[13] J. Wang, J. Polleux, J. Lim, B. Dunn, *J. Phys. Chem. C* **2007**, *111*, 14925 – 14931.
[14] C. Xia, J. Guo, Y. Lei, H. Liang, C. Zhao, H. N. Alshareef, *Adv. Mater.* **2018**, *30*, 1705580.
[15] P. He, M. Yan, G. Zhang, R. Sun, L. Chen, Q. An, L. Mai, *Adv. Energy Mater.* **2017**, *7*, 1601920.
[16] Z. Liu, P. Bertram, F. Endres, *J. Solid State Electrochem.* **2017**, *21*, 1 – 7.
[17] B. Zhang, Y. Liu, X. Wu, Y. Yang, Z. Chang, Z. Wen, Y. Wu, *Chem. Commun.* **2014**, *50*, 1209 – 1211.
[18] S. Jeong, J. Boo, *Thin Solid Films* **2004**, *447*, 105 – 110.
[19] A. Garcıa-Sánchez, E. Alvarez-Ayuso, *Miner. Eng.* **2002**, *15*, 539 – 547.

Manuscript received: December 26, 2017
Accepted manuscript online: February 12, 2018
Version of record online: February 23, 2018

